In: Hydroxyapatite: Synthesis, Properties and Applications ISBN: 978-1-62081-934-0
Editors: V. S. Gshalaev and A. C. Demirchan

Chapter VI

Morphology Control of Hydroxyapatite Crystal and its Aggregates

Wei Xia[1], Kaili Lin[2], Zhongru Gou[3] and Hakan Engqvist[1]
[1]Applied Material Sciences, Department of Engineering Sciences,
Uppsala University, Sweden
[2]Shanghai Institute of Ceramics, Chinese Academy of Sciences, China
[3]Zhejiang-California International Nanosystems Institute, Zhejiang University, China

1. Introduction

Hydroxyapatite ($Ca_{10}(PO_4)_6(OH)_2$, HA or HAp) is well known as a biomedical material for hard tissue repair and regeneration. HA can integrate in bone structures and support bone ingrowth, without breaking down or dissolving. HA is also a thermally unstable compound, decomposing at temperatures from about 800-1200°C depending on its stoichiometry. As a bioceramic, dense HA does not have the mechanical strength to enable it to succeed in long term load bearing applications.

Several other applications of hydroxyapatite are also interesting, such as drug/gene delivery, gas sensor, heavy metal ion adsorption, chromatography, catalyst, and photoelectric. The morphology, structure and size of hydroxyapatite crystal and aggregates would influence the performance in above applications. For example, rod-like, wire-like and sheet-like HA particles have a stronger molecular adsorption property due to the increased surface area, while HA nano-rods, nano-wires and nano-sheets can also be used for mechanical reinforcement to fabricate bio-composites because of their excellent mechanical properties. The hollow nano-structured HA microspheres can be used as drug-delivery system because of their high drug loading and favorably controllable release properties.

Many different methodologies have been proposed to prepare hydroxyapatite particles with different morphologies, such as plate-like (or sheet-like), needle-like, rods, spheres, core-shell structure, rods, whiskers, fibers, and “flowers” in micro- and nano- size. The most common strategies of controlling morphologies based on the above methods are to use templates that could direct crystal growth and the assembly of its aggregates. The templates

could be "soft materials," such as surfactants and biomoleculars, or "hard materials," such as calcium carbonates, calcium phosphate and calcium silicates. The mechanisms behind the template-directing processes are different. Another interesting strategy of morphology control is the self-assembly without any templates, such as biomineralization and mineralization, which are known as wet chemical routes.

In this chapter, we will summarize the recent studies of morphology control of hydroxyapatite with and without templates and discuss how templates direct the formation of HA particle and the possible mechanism of the self-assembly of HA. The applications of HA particles with different morphologies will be also discussed.

2. Morphology Control without Any Templates

Several techniques have been used to synthesize hydroxyapatite. These techniques can be mainly divided in two ways, solid-state reactions and wet process. The wet technique could include precipitation, hydrothermal, sol-gel and hydrolysis of other calcium phosphates, which could be regarded as "hard template." The usage of surfactants, such as urea; glycine; formamide; examethylenetetramine; sodium dodecyl sulfate; and organic moleculars, such as hexadecyltrimethylammonium bromide, amino acids, protein, monosaccharide, which could be regarded as "soft template," are to modify the wet process to prepare hydroxyapatite with morphology, stoichiometry, ion substitution or the degree of crystallinity required for a specific application. Other methods, such as microwave irradiation, freeze-drying , mechanochemical method , emulsion processing , spray pyrolysis, and ultrasounds can also be used to modify the preparation of HA particles.

In general, natural and synthesized hydroxyapatite crystals or particles are always plate-like (or flake-like) and thin because they grow elongated along the c-axis of the HA crystal [13, 67, 75]. Another explanation is that octacalcium phosphate (OCP) is the precusor of HA crystals, which grow along an OCP transition phase. OCP crystal itself is plate-shaped [88]. Because the surface energy of OCP is lower than that of HA, the energy barrier for nucleating HA is higher than that for OCP. Thus, HA prefers to grow along the OCP layer. B. Viswanath et al. developed a general methodology to illustrate the reason for the formation of plate-like HA, showing that the surface of lowest energy is the prism plane (100). They strongly recommend that the plate-like shape of OCP and HA is mainly due to the chemical driving force at which OCP or HA forms falls in the layer-by-layer growth zone. The relatively low temperature and neutral pH value favor the growth of two dimensional nanostructures associated with a low chemical driving force [91].

Needle-shaped HA crystals are also common structures, found in both tooth enamel and when prepared in a precipitation method. The preferred orientation gives rise to an oriented growth along the c-axis and a needle-like morphology. Previous studies [73, 9, 8] showed that polyglutamate could be absorbed on the hydrated layer of the OCP (100) face and phosphoryn could be preferentially adsorbed on the (100) face of apatite. In the enamel, the incorporation of F ion linearly increases its length via the c-axis. M. Andres-Verges et al. reported that the hydrothermal method could be used to synthesize needle-like HA particles, but the temperature and pH value of the reaction medium would influence the length and diameter of HA particles [90]. The carbonate substitution was shown to cause a reduction in crystallinity

and change in the shape from needle-like to rod-shaped to plate-like (equi-axed) crystals [63, 4, 87]. Koutsoukos et al. reported that the presence of chloride ions in the crystallizing medium favored the formation of plate-like HA crystals when a large amount of precipitation took place [37]. Zhang et al. tried to modulate the morphologies of HA particles with partial substitution of fluoride ion [102]. In their study, HA could be from prickly spheres, whisk brooms, flowers, dandelions, and nanofibers to ultralong nanoribbons. One main reason is the usage of glutamic acid, which adsorbs on HAp crystal surfaces through electrostatic attraction and hydrogen bonds, and possibly influences the morphological development of HA crystals. However, fluoride ion did have the effect on the morphology of HA. With the low F concentration (0.01g NaF in 150 water), spherical particles composed with needle-like apatite were obtained. When F concentration was increased, whisk-broom-like and dendritic particles appeared. More concentrated fluoride solution decreased the number and length of whiskers in the ends of the brooms, and the round handle of the broom gradually evolved into a prismatic one. Actually, it is not just because of the influence of fluoride, but the combined effect of fluoride and glutamic acid. Huang et al. reported Eu ion could influence the growth of HA crystals in the size and the ratio of length [23]. When the doping of Eu ion was 7.5%, the smallest ratio of width to length of HA crystals was obtained. The possible reason is that the substitution of Ca by Eu inhibited the crystal growth along the active plane.

Simulated body fluid (SBF) is a popular solution used to synthesize HA material. There are normally two ways to precipitate HA particles from the SBF, adjusting pH value and increasing temperature. Kobayashi et al. reported morphology variations of HA crystals via SBF based solutions [36]. If the pH value was adjusted to 6.5, phosphate-rich needle-like HA nanocrystals were precipitated at 38 °C. When pH value increased to 7.0, a nanosheet structure with (110) surfaces was steeply grown. If the temperature reaches 160°C, HA rods and plates in micormeter have been prepared in the solution with pH value of 7.0 and 7.4, separately. It is assumed that the adsorption of phosphates to the specific faces inhibits the growth of HA crystals and changes its morphology to low-dimensional forms. Bouyer et al. also found the morphology and size of HA particles are sensitive to the reaction temperature, and also to the reactant addition rate [7]. The pH value at the end of synthesis is a key parameter for determining the purity of the synthesized HA nanocrystal. A critical temperature (60°C) could be used to define HA particle in monocrystalline or polycrystalline in their system.

Kumar et al. reported that HA was synthesized via a wet chemical route using calcium hydroxide andortho-phosphoric acid [39]. The reaction temperature was found to affect the final morphologies of HA particles. Needle-like nanoparticles with a high aspect ratio were obtained at 40°C, while spherical particles were obtained when the precipitation temperature was increased to 100 °C. The analysis indicated that the supersaturation level of the reactants, especially the concentration of Ca^{2+} ions, played a predominant role in the precipitate morphology for the acid-base reaction. In certain cases, the usage of salts of week acid could affect the morphology of HA agglomeration. Yang et al. reported that potassium sodium tartrate tetrahydrate and trisodium citrate favored the assembly of spherical HA agglomeration with nanosheets and nanorods [96]. However, the mechanism behind it is not clear. The sol-gel method has also been introduced to prepare HA particles. The crystalization of sol-gel derived HA has much lower activation energy, and plate-like particles were always obtained as reported by A. Milev et al. [54]. The diffusion of ions would affect the crystalization of HA. Lu et al. demonstrated hexagonal HA rods could be obtained on the

surface of TiO_2 nanotubes array, while only plate-like HA crystal could be formed on a flat surface under a hydrothermal condition [49]. HA microspheres attract a lot of attention because of their potential applications in carriers, fillers, environmental protection, tissue engineering and chromatography [89, 77, 56, 11, 76, 82]. The only way of preparing HA microspheres without any surfactants, polymers and "hard" templates, such as calcium carbonate and calcium phosphates, is the spray technique, including spray drying, flame spray, and plasma spray, which is induced by the progress of gaining the lowest surface free energy when HA slurry is sprayed out [50]. If using this technique, the preparation of HA slurry, the spray temperature and post-treatment are very important. The obtained HA spheres normally have a large distribution in size, and the microstructure is difficult to control. Long HA fibers can be prepared using electrospinning method. Wu et al. reported that the HA fibers could be 10mm in length and 10-30μm in diameter, and the grain size of HA was around 1 μm in fibers [92]. Polymers were normally used to adjust the viscosity of the precursor of HA.

3. Soft-Templated HA Preparation and Properties

The controlled formation of HA minerals within organic or polymeric matrices is successfully used by nature to design biological materials. Many of the mineralized HA-based tissue formed by organisms in mammal animals have superior microstructures and mechanical properties. Therefore, templates have been used to mimic their design principles during the fabrication of synthetic HA materials.

In nature, nanoscale or microscopic vesicles often act as vehicles for ion transport and provide the microenvironment to promote controlled mineral nucleation and assembly. It is well believed that the matrix vesicles released by the osteoblast plasma membrane in bone tissue play an important role in the mineralization of the extracellular matrix and the formation of bone [52]. Numerous reports have shown that proteins and peptides, which have a high negative charge, inhibited the nuclear formation and crystal growth of HA, [10, 66, 62] and the HA-inhibiting activity of these proteins and peptides was reduced by modification of their phosphate group or carboxyl group [6, 25]. It is also shown that acidic proteins labeled with fluorescein were preferentially adsorbed on the (100) face of HAp crystal [19]. More recently, Matsumoto et al. studied the interaction between HA nanocrystals and a variety of amino acids in order to investigate the effect of amino acid on the crystallinity and the solubility characteristics of HA in the HA-synthesizing condition [53]. The HA synthesized in the presence of glycine (HA-Gly), serine (HA-Ser), aspartic acid (HA-Asp) and glutamic acid (HA-Glu) showed poor crystallinity compared with HAp synthesized in the absence of amino acid (HA-con). It is also demonstrated that the amino acids are adsorbed on the surface of HA. Furthermore, the solubility of these HA increased significantly compared to HA-con. However, other amino acids (i.e., proline, alanine, hydroxyproline, threonine, methionine, histidine) did not affect the crystallinity and morphology of HA and had no significant change in their solubility. These investigations suggest that the crystallinity and the solubility of synthesized HA are different, owing to the variation of amino acids in the HA synthesizing condition.

On the other hand, natural hydrogels, such as collagen, are the structural scaffolds in bone tissue, and it is possible to formulate synthetic hydrogels with similar elasticity and water retention ability. Hydrogels can be easily assembled in three dimensions while displaying multiple functional domains, and their polymerization chemistry allows the incorporation of polar ligands that mimic the acidic matrix proteins regulating mineral growth [3].

Song et al. have developed a template-driven nucleation and mineral growth process for the high-affinity integration of HA with a polyhydroxyethylmethacrylate (pHEMA) hydrogel scaffold [72].

A mineralization technique was developed that exposes carboxylate groups on the surface of cross-linked pHEMA, promoting high-affinity nucleation and growth of HA on the surface, along with extensive calcification of the hydrogel interior. Robust surface mineral layers a few microns thick can be obtained via a urea-mediated process. The same mineralization technique, when applied to a hydrogel that is less prone to surface hydrolysis, led to distinctly different mineralization patterns, in terms of both the extent of mineralization and the crystallinity of the apatite grown on the hydrogel surface. This template-driven mineralization technique provides an efficient approach toward bonelike composites with high mineral-hydrogel interfacial adhesion strength [70]. More recently, they used the (pHEMA) hydrogel as a versatile template for the urea-mediated surface mineralization and integration of HA with the substrate [71].

Two-dimensional outward growth of circular HA mineral domains from multiple nucleation sites was observed on the composite surfaces when heating urea-containing solution from room temperature to 95 °C and then maintaining for 10 h. Strong adhesion between the organic and inorganic layer was achieved for hydrogels functionalized with either carboxylate or hydroxy ligands. When extended mineralization was applied, the circular mineral domains eventually merged and covered the entire hydrogel surface with a final mineral layer several microns thick. The mineral-nucleating potential of hydroxyl groups identified in this study broadens the design parameters for synthetic bonelike composites and suggests a potential role for hydroxylated collagen proteins in bone mineralization.

Similarly, the phase separation can be used to create liquid vesicles inside the dense hydrogel matrix formulated to provide specific sites for the attachment of Ca ions and template for the crystallization of nano-HA. For example, Liu et al. combine both aspects into a seamless process to develop hierarchical structures in which the organic and inorganic phases are integrated at the nanoscale, while the mineral particles assemble into well defined microscopic structures leading to high mineral concentrations [45]. They have shown how current-assisted diffusion can be used to mimic vesicle-mediated mineralization in dense hydrogels.

The direct electric-current-assisted diffusion can promote the transport of Ca^{2+}, PO_4^{3-}, HPO_4^{2-}, and OH^- ions into a dense hydrogel matrix in the current-assisted diffusion setup. The use of pHEMA hydrogels resulted in the formation of micrometer-sized hollow microspheres of HA precursors.

Their size is very uniform and changes inversely with the hydrogel concentration. Mineral nanofibers (5-20 nm wide, 200 nm long) can be observed growing from the surface of these spheres into the hydrogel, while short and broader lamellar nanoparticles (up to 50 nm wide) grow toward the interior.

The fibers and lamellae are formed by the assembly of amorphous and crystalline nanodomains (5-20 nm in size). Such biomimetic mineralization process is helpful to clarify some poorly understood aspects in the crystallization of apatite and the origins of the transition between amorphous and crystalline inorganic phases during bone formation. Urea is usually used to catalyze the nanosized HA precipitation by increasing the pH value of the medium owing to the NH_3 formed by the hydrolysis of urea at an increased temperature condition. [29]

Aizawa et al. used urea as catalyzer for preparing HA fibers. The Ca-, P-containing starting solution was refluxed at 80 °C for 24 h to form OCP via $CaHPO_4$ and then the resulting OCP was converted into HA by refluxing at 90 °C for 72 h [2]. The pH in the solution increased from 3 to 8. The resultant fibre-shaped particles are 60μm to ~100μm with long-axes. High-resolution transmission electron microscopy observation confirmed that the apatite fibres were of single crystals with the *c*-axis orientation parallel to the long axis of the fibre.

Although uniform fibrous HA can be obtained by homogeneous precipitation below 100 ^oC using urea as the pH control agent, it is then generally calcium-deficient, with relatively low crystallinity and a low aspect ratio. Furthermore, the poor dispersibility of these whiskers due to entanglement or agglomeration becomes a problem when mixing with matrix materials. In general, both long and uniform HA whiskers, i.e., with controlled morphology and composition, are difficult to obtain by most commonly used methods because structure and properties are very sensitive to the preparation conditions, and both crystallinity and thermal stability are commonly inferior. Compared with the additive urea, which is used to raise the pH to drive nucleation and growth of HA crystals, acetamide has a low hydrolysis rate under the required hydrothermal conditions. This allows better and easier control, giving rise to rapid growth of whiskers at a low supersaturation. Long and uniform HA whiskers of mean length of 60~116 μm with high crystallinity, controlled morphology and high aspect ratio (68~103) could be synthesized by hydrothermal homogeneous precipitation using acetamide [101]. Such whiskers are favorable for their improved bone bonding and bioactivity, as well as their mechanical properties. Whiskers were slightly Ca-deficient with Ca/P = 1.60~1.65, with the preferred direction of growth along the c-axis. Variation of acetamide concentration did not affect the constitution, the crystallinity or the crystal growth habit. Nagata studied the effect of methanol on the morphology of HA crystals from a precursor HA slurry under hydrothermal conditions in the presence of methanol [58]. It was found that the products obtained from slurries without methanol were rod-like or granular crystals, about 20 to 100 nm in size. Addition of methanol to the slurries caused an increase in the ratio of plate-like crystals to rod-like crystals or granular crystals. When the weight of methanol added was equal to the weight of the slurry, only plate-like crystals 20 to 200 nm in size were obtained. The morphology of the products was influenced by the amount of methanol added to the slurry. XRD patterns of oriented products indicated that the plane grown selectively was the α-plane of the plate-like crystals. Furthermore, the variation of the morphology can be attributed to the adsorption of methanol on the surface of the HA nuclei inhibiting the crystal growth along a particular axis according to the DTA analysis. The morphological control of HA crystals modulated by amphiphilic molecules has been reported previously by some researchers. Yan et al. report a two-step synthetic method, using the surfactants as regulator of the nucleation and crystal growth of nano-HA at room temperature and at 150^oC, respectively [95].

The precipitates obtained at room temperature were fibrous polycrystals, but the CTAB-involved samples transformed to nanorods (150 nm×10 nm) with uniform morphology after hydrothermal treatment. The PVA-involved sample simply gave aggregates. The high temperature and pressure of hydrothermal treatment could exert both effects on the final product. Firstly, they might cause some fibers to aggregate, but the interaction between the aggregates is so weak that they tend to dissolve in the aqueous system. Secondly, they might raise the solubility of HA to some extent and accelerate the dissolution and crystallization process. Since the crystallization process is under critical control of CTAB, the resulting HAs were invariably nanorods. The behavior of CTAB was considered to orrelate with the charge and stereochemistry properties.

In an aqueous system, CTAB would ionize completely and result in a cation with tetrahedral structure. Meanwhile, the phosphate anion is also a tetrahedral structure. The charge and structure complementarity endows CTAB with the capability to control the crystallization process. While in the PVA-involved case, things are different. It is a nonionic surfactant so that the electrostatic interaction is impossible, and the van-der-Wall's interaction would be the major force. Perhaps in the hot and strong environment, the interaction is too weak so the PVA could exert little influence on the products. Liu prepared the HA nanorods successfully at 85°C in water bath in the presence of suitable ethanoic acid, cetylrimethylammonium bromide (CTAB) and PEG 400 [47]. The as-made nanorods have a diameter of 50–80 nm and a length of 0.5–1.2 μm. On the other hand, in the presence of CTAB only needle-like structure is obtained. In the absence of both CTAB and PEG 400, particles are obtained [47]. In the presence of CTAB, cyclohexane and sodium nitrate, HA nanofibers with 5–8 nm in diameter and 160–220 nm in length are obtained [48]. These experiments suggest that the additions of CTAB, PEG 400, NH_3OH and ethanoic acid are crucial for the formation of the nanorods. The growth mechanism of HA nanorods could be explained by a soft template. The effect of CTAB on the formation of HA nanorod is as follows: (1) PEG is a non-ionic surfactant. The PEG monomer can easily form long chain structures in aqueous solution [34]. (2) In an aqueous system, CTAB would ionize completely and result in a cation with tetrahedral structure [95]. In addition, CTAB solution with a certain concentration enhances the rod yield and has a tendency to form elongated rod-like micellar structures [81], which possibly served as a soft template, assisting in the formation HA nanorods. (3) The phosphate anion is also a tetrahedral structure. Thus, it is proposed that the charge and structure complementarily endows CTAB, PEG and pH of solution with the ability to control the crystal growth process. Moreover, Sauer et al. applied ionophores to control concentration with triblock copolymer vesicles and precipitate HA nanorods [69]. It is believed that this concept of combing artifical block copolymer membranes with natural membran proteins holds great potential for biomimetic mineralization. Bose et al. successfully prepared the HA nanoneedles 30~50 nm in size with a surface area of 130 m^2/g and particle size between with shape and spherical morphology [5]. These nanocrystalline HA powders were synthesized using the reverse micelle-processing route in the cyclohexane/water system, mixed poly(oxyethylene)$_5$ nonylphenol ether (NP-5) and poly(oxyethylene)$_{12}$ nonylphenol ether (NP-12) as the surfactant phase, and a solution of $Ca(NO_3)_2$ and H_3PO_4 was used as the aqueous phase. It was found that experimental conditions such as aqueous/organic phase volume ratio, pH, aging time, aging temperature, and metal ion concentration in the aqueous phase affected the crystalline phase, surface area, particle size, and morphology of HAp nanopowders. With the use of this technique,

nanopowders were prepared with different morphology depending on the reaction parameters. Similarily, Sadasivan used the reverse micelles of calcium bis(2-ethylhexyl)phosphate ($Ca(DEHP)_2$) to synthesize HA nanostructures from a reaction mixture initially containing a water-in-cyclohexane emulsion of $Ca(DEHP)_2$, ammonium hydrogen phosphate, and triblock copolymer, P123 [68].

Bundles of DEHP-coated amorphous calcium phosphate nanofilaments, 2 nm in width and >300 μm in length were formed in the oil layer of a phase-separated reaction mixture prepared at a [Ca]: [PO_4] molar ratio of 1:1 and pH of 8.2. The nanofilament bundles were stable in the reverse micelle phase up to around 5 days, after which they transformed into 5-nm-wide surfactant-coated HA nanorods.

In contrast, similar experiments at a higher supersaturation level (pH = 9, [Ca]: [PO_4] = 1.66) produced discrete nanofilaments (100-500 ×10-15 nm in size) that consisted of a linear superstructure based on the side-on stacking of surfactant-coated amorphous calcium phosphate nanorods.

Chitosan is the rarely naturally derived cationic polysaccharide. Some investigation suggested that this polyelectrolyte modulates the nanocrystalline HA particles in aqueous solutions. For example, Li et al. reported that the nano-HA could be mineralized in situ in the chitosan–pectin polyelectrolyte complex (PEC) network [40].

Especially, the pH value is the main factor to control the nucleation and growth of nHA crystal in chitosan–pectin PEC networks, because both the interactions' strength between nHA crystal and chitosan–pectin and diffusion rate of inorganic ions depend on the pH value of the reaction system.

The crystallite size of the nHA particles (L) from the (002) face is calculated by Scherrer's equation coincided to the particle length. Chitosan–pectin networks lead to nHA crystallite sizes in the range 16.4–8.2 nm for the [002] directions. This size is very similar to the value of 18.6–16.4 nm for apatite from nature bone. The particle size distribution also seems narrow and uniform in all samples. Furthermore, nHA crystals are embedded in chitosan–pectin PECs network, and the needle-type nHA crystals, with a mean length and width of about 100 and 8 nm, respectively, can be observed. Furthermore, SAED analysis on the granulated aggregates region exhibit polycrystalline diffraction rings, which are identified as the crystallographic planes (112) and (002) of the HA crystals.

Wang et al. investigated that the HA nanoparticles with equivalent diameter about 20–40 nm precipitated in distilled water or ethanol or the mixture of them in the presence of different dispersants such as ethanolamine, citric acid and polyethylene glycol (PEG-12000) were spherical or close to spherical in shape, with different sizes and dispersibility [84].The dispersant could prevent the products from aggregating during synthesis process. It is interesting that the temperature of reaction was another important factor that influenced the morphology of nano-HA.

The HA nanoparticles prepared at 25°C, 40°C, 60°C, and 80°C had four different morphologies: sphere- and rod-like at 25 °C, sphere- or close-to- sphere-like at 40 °C, rod-like at 60 °C and bamboo-leaf-like at 80 °C. All of the diffraction patterns of the XRD patterns of HA powders revealed characteristic peaks of HA, except the one synthesized at 25 °C, which showed peaks of amorphous state. The patterns indicated that high reaction temperature was propitious to the crystallization of HA.

4. Morphology Control of HA Crystal and Its Aggregates Using "Hard Templates"

Recently, another approach, using hard-templates, such as calcium phosphate, calcium carbonate, calcium silicate, etc. as the precursors has been developed to delicately control the morphologies of HA from simple 0D morphologies to complicated 3D architectures. The merit of applying the hard-templates as precursors was attributed to facileness, low-cost and large-scale synthesis process.

In addition, the sizes and/or chemical compositions of the final HA products can be easily regulated by changing the conditions of the precursors. Therefore, the hard-template method provides a new platform for HA materials to be efficiently synthesized and manipulated. In this section, the morphology control of HA materials using solid precursors as the hard-template is summarized, and the possible morphology formation-mechanisms are also discussed.

Using the solid precursors as the hard-template to fabricate the inorganic materials with especial morphologies and/or chemical compositions has widely aroused attentions in material and device fields for several decades. Many researchers studied the synthesis of HA powders using the natural or synthesized calcium carbonate ($CaCO_3$) powders as the precursors under hydrothermal methods. Jokanovic et al. used the CaO powders calcined from the chicken eggs and $(NH_4)_2HPO_4$ solution as the calcium and phosphor sources, respectively [30]. After hydrothermal treatment, the precursors completely transferred into HA powders with agglomerated particles of 5-20μm, built up from particles of approximate 200 nm. In addition, the study also revealed that the hydrothermal treatment parameters, such as precursor and phosphor source concentration, temperature, pressure and reaction time played important roles in the crystal lattice parameters, crystallite size, crystallinity, composition, microstructure and specific surface area of the products.

Yang et al. prepared plate-like carbonated hydroxyapatite (CHA) crystals with a width-size of 100-200nm and a thickness of approximately 25nm via hydrothermal conversion of fine $CaCO_3$ powders milled from oyster shells in $(NH_4)_2HPO_4$ solution [97]. The hydrothermal conversion allowed ionic exchange without destroying the morphology of the raw oyster shell powders based on the reaction equation:

$$10CaCO_3 + 6(NH_4)_2HPO_4 + 2H_2O \rightarrow Ca_{10}(PO_4)_6(OH)_2 + 6(NH_4)_2CO_3 + 4H_2CO_3 \quad (1).$$

In the conversion process, the CO_3^{2-} ions incorporated into the HA crystal lattices, which resulted in CHA products. Furthermore, the dense structures of piece-shaped and screw-shaped HA were created by hydrothermal conversion of conch and clamshells according to Eq. 1. The conversion process was accelerated at higher temperatures, and the thickness of the HA layer around precursors increased with the increase of the conversion time.

The average fracture stress of the obtained samples reached 137-218MPa, which is close to that of compact human bone. This indicated that the converted shell samples can be used as implants in load-bearing applications. Yoshimura et al. prepared the plate-like HA crystals via hydrothermal treatment of the synthesized calcite in H_3PO_4 solution based on the dissolution/precipitation mechanism, followed by nucleation and growth on the surface of calcite crystals [99].

Based on Eq. 1 under hydrothermal transformation, Rocha et al. used cuttlefish bones with highly channelled structures as the precursors to synthesize HA scaffolds. The transformation completed quickly after 9 h at 200^{o}C and no intermediate products remained. After conversion, the initial structure of the cuttlefish bones was preserved, which exhibits micropore size of ~80μm in width and ~100μm in height. The HA crystallites formed had a size of nanoscale (~20-50nm), similar to the size of bone-like apatite, and were strongly resembled into bi-layered nano-structures [65, 64].

If the phosphor sources of $(NH_4)_2HPO_4$ solution were replaced by $NH_4H_2PO_4$, the HA crystallites in the products were in plate- and needle-like shapes [28]. Corals were also used as the precursors to synthesize HA scaffolds with interconnected macroporous structures [22]. The SEM observation showed that the both tablet and stacks-of-tablets morphologies similar to the original nacre structures were preserved after conversion of the nacre pieces (2-4 mm) in $(NH_4)_2HPO_4$ solution [100].

The conversion of silicate (45S5) and borosilicate glasses (partially replacing the SiO_2 by B_2O_3 in the silicate-based 45S5 bioactive glass) to HA in dilute K_2HPO_4 solution (0.02M) at near body temperature was investigated by Huang's group [24]. After conversion, the layered structures of HA assembled by sheet-like particles formed in situ. In addition, the higher B_2O_3 content of the glass produced a more rapid conversion to HA and a lower pH value of the phosphate solution. Furthermore, the hollow HA microspheres were fabricated by conversion of solid microspheres of a Li_2O-CaO-B_2O_3 glass in K_2HPO_4 solution [18, 1, 24, 85]. The effect of the temperature, K_2HPO_4 concentration and pH of the solution on the diameter (d) of the hollow core normalized to the diameter (D) of the HA microspheres; the surface area and the pore size of the microsphere wall was studied in detail. The studies showed that the pH had little effect, while the concentration of the solution had a marked effect on d/D, surface area, and pore size, whereas temperature markedly influenced d/D and pore size, but not the surface area. On the other hand, the shell size of the HA increased with the increase of the CaO contents. When the weigh percentage of CaO increased up to 30%, the HA microspheres showed a compact other than hollow structure. The obtained hollow HA microspheres possessed high surface area (135m^2/g) and good rupture strength (1.6±0.6 MPa). The consequences of these results for potential application of these hollow HA microspheres as devices for local delivery of proteins, such as drugs or growth factors, are discussed. These hollow HA microspheres might be useful as devices for drug or protein growth factor delivery or as scaffolds for engineered tissues [98].

As the precursor phases during the in vivo mineralization, the amorphous calcium phosphate (ACP), octacalcium Phosphate (OCP), monetite ($CaHPO_4$, DCP) and dicalcium phosphate dihydrate (DCPD), etc. have been widely used as the precursors of the hard-templates to synthesize and morphology control of the HA crystals. Tang et al. have discovered that only when the starting nanoparticles were aggregates of nanospheres with HA cores and ACP shells, would highly ordered HA architectures be formed with the help of glycine (Gly) and glutamate (Glu) [78]. These finding provide evidence for a new mechanism for assembly of biominerals in which ACP functions by linking HA nanocrystals while they assume parallel orientations and is then incorporated by phase transformation into HA molecules that rigidly link HA nanocrystals in larger fused crystallites. The biologic molecules regulate the assembly kinetics and determine the structural characteristics of the final HA architecture. Pan et al. further observed that the transformation from ACP to HA takes place in about one hour. During the transformation, the nucleation occurs preferably at

the surface of ACP spheres. The embedded/adhered crystallites on the ACP surface would not allow the crystallites to rotate their orientations and/or relocate from their relative positions. This gives rise to the formation of HA spherulites [59]. Recently, they have successfully performed a bio-inspired enamel repair experiment via Glu-directed assembly of apatite nano particles. Therefore, once again, the investigations highlighted the importance of biomineralization principles—the nano assemblies of building blocks, the regulation effect of organic species and the template crystallization [41]. The study of Kim et al. also showed that the more excess calcium ions exist in the calcium-rich solution, the more rapidly HA crystallization from ACP occurred, and the Ca/P molar ratio of the finally obtained precipitates increased to reach the stoichiometric value of 1.67 [35]. The similarity of the apatite layer in OCP and the apatite structure in HA provides geometrically favorable conditions for phase transformation from OCP to HA. The tranformation follows a dissolution–precipitation process in aqueous environment.[15] Leng's group also observed the mechanism of solid-state transformation phenomenon from OCP to HA by electron beam irradiation in transmission electron microscopy (TEM) [93]. The dicalcium phosphate dihydrate ($CaHPO_4 \cdot 2H_2O$, brushite) are thermodynamically unstable under pH values greater than 6–7 and undergo transformation into more stable calcium phosphates (e.g., HA) via the dissolution–precipitation mechanism [38]. After soaking the plate-like brushite in alkaline solutions at pH 10.8, the similar plate-like HA agglomerate, with a size around 30μm, composed of fine particles (<1μm) were obtained. The study showed that the conversion crucially depended on temperature and pH. In addition, the addition of Ca^{2+} ions into solution caused the acceleration of the conversion process [74]. Monetite (dicalcium phosphate: $CaHPO_4$, DCP) was found to be a good precursor of hard-template for nanoscopically controlled HA crystals. Nanoscale needles, fibers, and sheets of HA could be selectively prepared through the conversion the DCP precursor in an alkali solution by varying the pH and ion (Ca^{2+} or PO_4^{3-}) concentrations via the balance of the topotactic solid–solid phase transition and dissolution–crystallization processes. An oriented array of bundled nanoneedles of HA elongated in the c-axis was obtained under a highly basic condition at pH 11–13. The ordered architecture originated from the spatially periodic nucleation of HA seeds on the DCP surface through topotactic solid–solid transformation. Long HA fibers were observed under a relatively mild basic condition at pH 9–10. The fibrous morphology evolved from the nanoneedles produced by the solid–solid transformation with the elongation of the c-axis through a dissolution-precipitation route. Flaky HA nanosheets consisting of a parallel assembly of nanoneedles were observed with an excess amount of phosphate ions under mild basic conditions. The presence of phosphate ions suppressed the solid–solid transformation and promoted the formation of a two-dimensional structure with the dissolution-precipitation process. Furthermore, the hierarchical architecture of including the macroscopic morphology and the nanostructures similar to those of the human bones and teeth could be controlled by regulation the pH values [27]. Ma et al. synthesized flowerlike and bundlelike monetite consisting of nanosheets by a one-step microwave assisted method using $CaCl_2 \cdot 2.5H_2O$, NaH_2PO_4, and sodium dodecyl sulfate (SDS) in water/ethylene glycol (EG) mixed solvents. After immersion in NaOH solution at 60°C, the monetite transformed to HA phase, and the morphologies were well maintained [51]. The hierarchical architectures of the nanostructured HA could also be successfully achieved by the hard-template transition associated with the specific interaction of the organic molecules. The organized nanostructures of HA were

produced using a novel preparation route through the topotactic transition of dicalcium phosphate dihydrate (DCPD) containing gelatin molecules.

A nanoscale texture of dicalcium phosphate (DCP) was formed by the dehydration of DCPD prepared in gelatin gel containing phosphate ions. A three-dimensionally oriented framework of HA consisting of ca. 20 nm grains was prepared by a rapid hydrolysis of the nanotextured DCP with a sodium hydroxide solution. However, hydrolysis at a low pH (pH 10.0) using an NH4OH solution produced aggregates of nanofibrous HA. The hierarchical architectures of the nanostructured HA providing a high specific surface and macroscopic pores would be applicable for various biomedical applications [20].

The carbonated apatites (CHA) with different carbonate contents were prepared by the conversion of monetite ($CaHPO_4$, DCP) in solutions with a Na_2CO_3 concentration ranging from 0.001 to 0.075mol/L. The influence of the carbonate content in apatites on the adhesion and the proliferation of MC3T3-E1 osteoblastic cells were further investigated. The cell culture results showed that only the apatites with a carbonate content higher than 11% supported both high cell adhesion and proliferation [60].

The α-triclcium phosphate (α-$Ca_3(PO_4)_2$, α-TCP) and calcium silicate with good dissolution ability provide another precursor to modulate the morphology of HA crystals. After hydrothermal treatment the α-TCP powders, granules and scaffolds in aqueous solutions, the precursors will be transformed to nano- or micro-sturecuted HA materials with similarly macroscopical appearances [26, 83, 46].

Furthermore, through simply adjusting the reaction temperature and the concentration of Ca^{2+} ions under hydrothermal treatment of the α-TCP powders in aqueous solutions without using any surfactants or additives, the well developed HA crystals with different structures and morphologies (chrysanthemum-like HA microflowers, enamel-like HA microparticles, rectangle shaped HA microplates and HA microrods) could be obtained. The experimental results showed that different aggregation routes of HA nanorods that grow along the c-axis were the reason for the formation of various micro-structures and morphologies. Recently, a novel process has been developed to synthesize element-substituted HA with controllable morphology and chemical composition using calcium silicate as hard-template precursors in the absence of any surfactants and additives by Lin et al. [43]. In this work, the element-substituted HA powders with controllable morphologies and chemical compositions were synthesized via hydrothermal treatment of a calcium silicate precursor in phosphate solutions. With hydrothermal treatment of the calcium silicate hydrate (CSH) precursor in Na_3PO_4 solution, the HA nano-particles with diameters about 90 nm were obtained (Figure 1A). In contrast, when the crystalline calcium silicate (CS) powders were used as the precursor and the Na_3PO_4 solution was used as phosphorus source, the obtained HA powders consisted of nano-wires with lengths up to 2 μm and diameters about 100 nm (Figure 1B). Figure 1C illuminates that the obtained HA powders via hydrothermal treatment the crystalline CS powders in NaH_2PO_4 solutions had a smooth surface and ultra long sheet-like shape with thickness about 100 nm, widths 1~5 μm and lengths up to 20 μm, and almost no particles or rods were observed. The model of $Ca_9(PO_4)_6$ clusters (Posner Clusters) with positive charge could be applied to illuminate the effect of the different phosphorus sources on HA morphology development [61]. The $Ca_9(PO_4)_6$ clusters are considered the growth unit of HA crystals. The Ca^{2+} ions gradually dissolved from the calcium silicate precursors into the phosphate solution to form $Ca_9(PO_4)_6$ clusters. It is well known that hexagonal HA crystal has two types of crystal surfaces with different charges, positive on *a*- and *b*-surfaces and

negative on *c*-surfaces [33]. Usually, hexagonal HA crystals, which grow along the c-axis, are easily obtained because of a strong bond site for $Ca_9(PO_4)_6$ cluster in the [0001] direction, but not in the [1010] direction. The crystal growth is thus easier in the [0001] direction than in the [1010] direction. In the Na_3PO_4 solution, a large quantity of PO_4^{3-} ions were ionized into the solution. Therefore, there would be enough PO_4^{3-} ions to form Posner Clusters with Ca^{2+} ions dissolved from CS particles. The released Ca^{2+} ions were rapidly consumed, which resulted in quite a few Ca^{2+} ions remaining in the near of the surfaces of CS particles. According to the Cluster Growth Model for HA, Posner Clusters would attach to *c*-surfaces preferentially and the direction along c-axis developed quickly. Ultimately, the HA nano-wires were obtained. However, in the NaH_2PO_4 solution, the hydrolyzation of NaH_2PO_4 salts was greater than ionization. The major ions in the solution were $H_2PO_4^{-}$ and HPO_4^{2-} ions, and there were only small amount of PO_4^{3-} ions formed from the secondary ionization. Therefore, large amount of released Ca^{2+} ions were attached to the *c*-surfaces with negative charges, which resulted in less Posner clusters incorporated onto the *c*-surfaces. The growth of *c*-surfaces was limited, while the growth of *a, b*-surfaces was enhanced, leading to the aggregation of *a, b* planes.

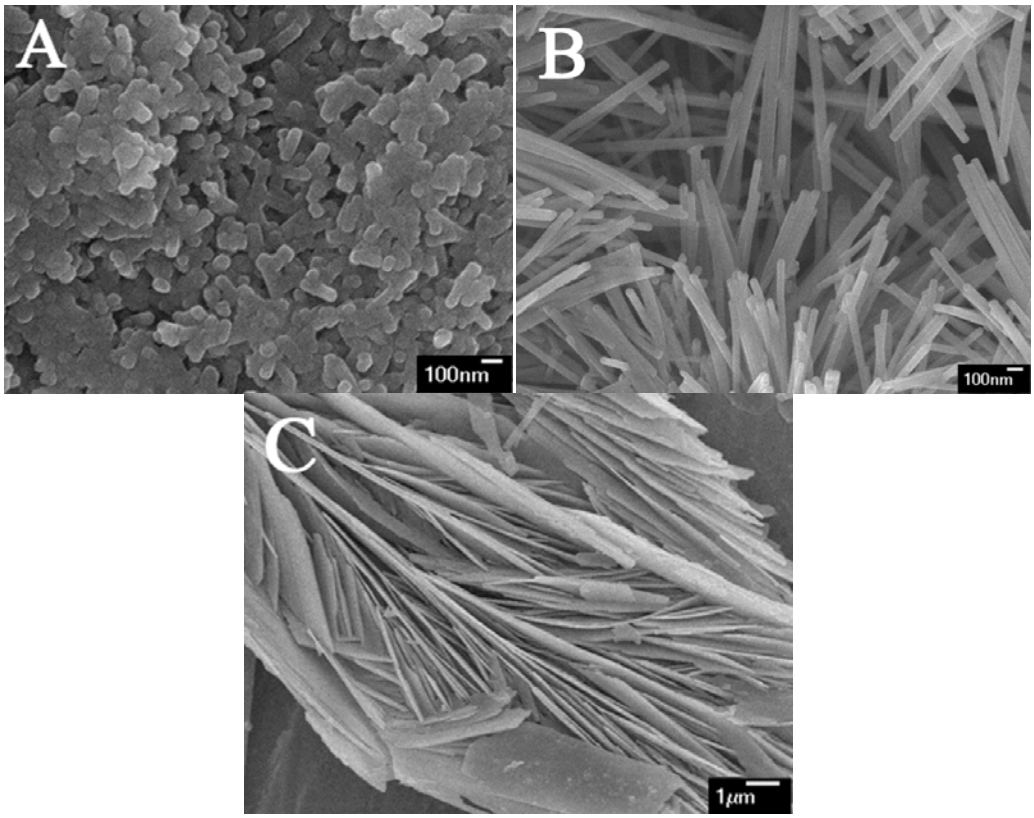

Figure 1. FESEM images of HA powders with different morphologies. A: nanoparticles (CSH as precursor, Na_3PO_4 as solution); B: Nanowires (CS as precursor, Na_3PO_4 as solution) and C: nanosheets (CS as precursor, NaH_2PO_4 as solution).

Ultimately, the HA nano-sheets were obtained. However, the morphology of the synthesized HA was nano-particles after hydrothermal treatment the CSH powders in Na_3PO_4 solution. This might be attributed to the crystal structure of CSH itself. It is well known that the CSH is a poorly ordered phase with layered structures. The layer consists of a central Ca-O part sandwiched between parallel silicate chains [79]. When hydrothermal treatment in phosphate solution, the HA crystal formed accompanied with the split of the sandwiched layers and silicate chains of the CSH into the short fragmentations. In this situation, HA crystals were formed on these fragmentations, resulting in the particle-like products. At the same time, through regulating the chemical compositions of the precursors and the reaction ratio of the precursor/solution, the HA crystals substituted by different kinds and amount of elements (such as Si, Na, Mg, and Sr, etc.) could be easily obtained.

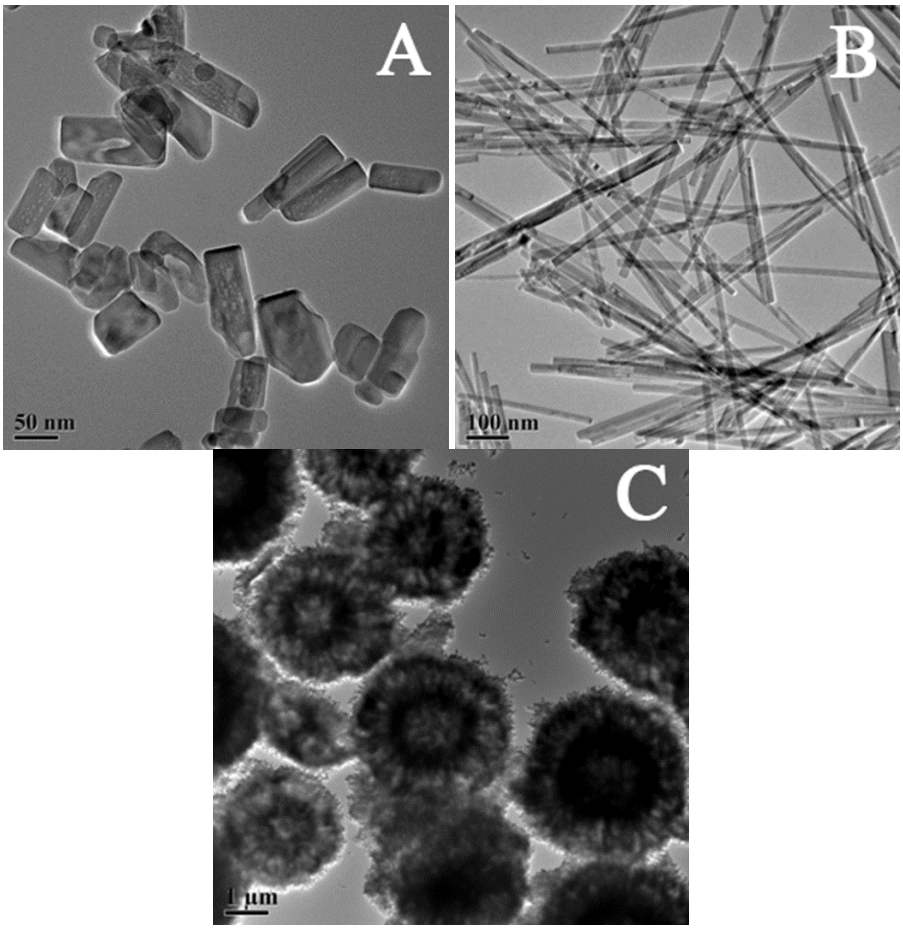

Figure 2. Morphologies of the HA nanoparticles, nanowires and nano-structured hollow HAp microspheres transformed from $CaCO_3$ nanoparticles, $Ca_6(Si_6O_{17})(OH)_2$ nanowires and hollow $CaCO_3$ microsphere precursor, respectively.

Recently, Lin et al. also developed a facile strategy to delicately control the morphologies of HA materials from simple 0D morphologies to complicated 3D architectures using hard-precursors with similar structures, which provided a new platform for HA materials to be efficiently synthesized and manipulated [42]. The HA nanopartilces, nanowires and hollow

nano-structured microspheres (Figure 2) were successfully synthesized easily via hydrothermal treatment of the similar structured precursors of calcium carbonate ($CaCO_3$) nanoparticles, xonotlite [$Ca_6(Si_6O_{17})(OH)_2$] nanowires and hollow $CaCO_3$ microspheres in Na_3PO_4 solutions, respectively. In addition, their sizes can be easily regulated by changing the template conditions. With hydrothermalization of the precursors in phosphate solution, the surface erosion occurred on the precursors, accompanied by the release of the Ca^{2+}, CO_3^{2-} (from $CaCO_3$ precursor) and Ca^{2+}, SiO_3^{2-} (from xonotlite precursor) ions into the solutions.

With the increase of the ion-release amount, the concentration of the Ca^{2+} and PO_4^{3-} reached over saturation and the HA nucleated on the eroded precursor surfaces. During this process, the precursors themselves played the roles of the Ca^{2+} ion source and the HA crystal nucleation sites. With the prolonging of the reaction periods, the ions released continuously and the HA crystals grew continually. Ultimately, the phases of the precursors disappeared and transformed into the final HA products. In this process, the morphologies of the precursors can be well preserved without destruction. At the same time, part of the Na ion came from the phosphate solution, and Si or carbonate ions released from the precursors were incorporated into the newly formed HA crystal lattices.

5. Application

HA is well known as a bioactive material used in hard tissue repair and regeneration. Other applications of HA are also interesting, such as drug/ gene delivery, gas sensor, heavy metal ion adsorption, chromatography, catalyst, and photoelectric. The performance of HA materials in the above applications depends on its crystal morphologies, particle sizes and three-dimensional (3D) architectures.

Porous and hollow spheres inherently favor drug and proteins delivery. High drug loading and slow release could be expected. HA microspheres have been studied as an injectable drug delivery systems aimed at periodontitis treatment and simultaneously initiating the osteointegration process. Amoxicillin, clavulanic acid and erythromycin were the antibiotics used in Ferraz's experiment [17]. A long-term sustained release with the effective dose was obtained, compared with using regular HA particles.

Emoto et al. tried to use resorbable calcium-phosphate microspheres loaded with an agent anti-angiogenic to treat tumors [16].

Their results suggest that targeting tumor vasculature in human uterine sarcoma using calcium phosphate microspheres might be more effective and safer than the treatment that employs an anti-angiogenic agent alone. Mizushima et al. examined spherical porous hydroxyapatite microparticles as carriers for protein and lipophilic drugs, such as interferon alpha (IFNa), testosterone enanthate (TE), and cyclosporin A (CyA). In the in vitro and in vivo results, these porous HA microspehres not only showed a sustained release but also a good injectibility [55].

Bovine serum albumin (BSA) with negative surface charge and lysozyme hydrochloride (LSZ) with positive charge were also used to study the protein release from HA spheres that have good affinity of both negative and positive substance in water solution. The release could last more than 2 weeks.

The slow release of BSA may indicate that these spheres could more easily adsorb negative protein [80]. Because HA nanoparticles are able to permeate the cell membrane and dissolve in the cell, they could also be a candidate for gene delivey. HA nanoparticles could be nonviral gene delivery systems, which protect DNA from the cytoplasmatic environment and enables it to go into cell nucleus. HA nanoparticles are more suitable as a gene delivery system than silica, quantum dots, carbon nanotubes and magnetic particles because they are soluble and less toxic. The rod-like, wire-like and sheet-like HA particles have a stronger molecular adsorption property due to the increased surface area [86].

HA nano-rods, nano-wires and nano-sheets can be used for mechanical reinforcement to fabricate bio-composites because of their excellent mechanical properties [12, 57, 14]. Dubey et al. pointed out that HA nanocrystal shape along with the optimal direction was important to strengthen the materials at nanoscale. Muller et al. reported that HA whiskers can increase the bending strength of calcium phosphate cements by 60%. Fibrous HA can be as a promising reinforcement for HA/polymer biodegradable bone substitutes, a constituent for porous HA ceramics or porous HA/-TCP composites, and a skeletal mesh with ion-exchange properties for filtration [92].

Because of high surface area and the affinity of certain ions and molecurs, porous and nano HA particles can be applied as a sorbent to remove toxic and hazard substance [21, 44]. Otherwise, HA foam was also studied as a catalyst for formaldehyde combustion at room temperature [94]. Porous hydroxyapatite beads and HA particles can also be as a matrix for the chromatography of both proteins and nucleic acids [32], but they are unsatisfactory with respect to flow rate, stability, and elution characteristics. HA has proved useful in the separation of IgG idiotypes that cannot easily be separated by other techniques [31].

References

[1] Ai F R, Yan H, YAO A-H, HUANG W-H and LI Y 2011 Preparation of Shape-Controlled Hollow Hydroxyapatite Microsphere at Room Temperature *Chinese Journal of Inorganic Chemistry* 27 2372-6.

[2] Aizawa M, Ueno H, Itatani K and Okada I 2006 Syntheses of calcium-deficient apatite fibres by a homogeneous precipitation method and their characterizations *J. Euro. Ceram. Soc.* 26 501-7.

[3] Barrera D A, Zylstra E, Lansbury P T and Langer R 1993 Synthesis and RGD peptide modification of a new biodegradable copolymer system: Poly(lactic acid-co-lysine) as an interactive, resorbable biomaterial *J. Am. Chem. Soc.* 115 11010-1.

[4] Bocciarelli D 1970 Morphology of crystallites in bone *Calcif. Tissue Int.* 5 261– 9.

[5] Bose S and Saha S K 2001 Synthesis and characterization of hydroxyapatite nanopowders by emulsion technique *Chem. Mater.* 15 4464-9.

[6] Boskey A, Maresca M, Ullrich W, Doty S and Butler W 1993 Prince CW.Osteopontin–hydroxyapatite interactions in vitro: inhibition of hydroxyapatite formation and growth in a gelatin–gel *Bone Miner* 22 147-59.

[7] Bouyer E, Gitzhofer F and Boulos M I 2000 Morphological study of hydroxyapatite nanocrystal suspension *J. Mater. Sci. Mater. in Med.* 11 523-31.

[8] Burke E M, Guo Y, Colon L, Rahima M, Veis A and Nancollas G H 2000 Influence of polyaspartic acid and phosphophoryn on octacalcium phosphate growth kinetics *Colloids Surf. B* 17 49-57.
[9] Chander S and Fuerstenau D W 1984 Solubility and intrfacial properties of hydroxyapatite:A review: in Missra DN(ed): Adsorption on and surface chemistry of hydroxyapatite *Plenum. Press* 29-49.
[10] Chen C and Boskey A 1985 Mechanism of proteoglycan inhibition of hydroxyapatite growth *Calcif. Tissue Int.* 37 395-400.
[11] Cho J S and Kang Y C 2008 Nano-sized hydroxyapatite powders prepared by flame spray pyrolysis *J Alloy Compd* 464 282-7.
[12] Corma A, Rey F, Rius J, Sabater M J and Valencia S 2004 Supramolecular self-assembled molecules as organic directing agent for synthesis of zeolites *Nature* 431.
[13] Dorozhkin S V 2007 Calcium orthophosphates *J. Mater. Sci.* 42 1061-95.
[14] Dubey D K and Tomar V 2009 Role of hydroxyapatite crystal shape in nanoscale mechanical behavior of model tropocollagen–hydroxyapatite hard biomaterials *Materials Science and Engineering C* 29 2133-40.
[15] Elliott J 1994 *Structure and Chemistry of the Apatites and Other Calcium Phosphates* (Amsterdam: Elsevier).
[16] Emoto M, Naganuma Y, Choijamts B, Ohno T, Yoshihisa H, Kanomata N, Kawarabayashi T and Aizawa M 2010 Novel chemoembolization using calcium-phosphate ceramic microsphere incorporating TNP-470, an anti-angiogenic agent *Cancer Sci.* 101 984-90.
[17] Ferraz M P, Mateus A Y, Sousa J C and Monteiro F J 2007 Nanohydroxyapatite microspheres as delivery system for antibiotics: Release kinetics, antimicrobial activity, and interaction with osteoblasts *J. Biomed. Mater Res. A* 81 994-1004.
[18] Fu H, Rahaman M N and Day D E 2010 Effect of process variables on the microstructure of hollow hydroxyapatite microspheres prepared by a glass conversion method *J. Am. Ceram. Soc.* 93 3116–23.
[19] Fujisawa R and Kuboki Y 1991 Preferenti al adsorption of dentin andbone acidic proteins on the (1 0 0) face of hydroxyapatite crystals *Biochim. Biophys. Acta.* 1075 56-60.
[20] Furuichi K, Oaki Y and Hiroaki Imai 2006 Preparation of Nanotextured and Nanofibrous Hydroxyapatite through Dicalcium Phosphate with Gelatin *Chem. Mater.* 18 229-34.
[21] Hammaria L E L, Laghzizila A, Barbouxb P, Lahlilb K and Saoiabia A 2004 Retention of fluoride ions from aqueous solution using porous hydroxyapatite Structure and conduction properties *Journal of Hazardous Materials B* 114 41–4.
[22] Hu J, Russell J J and Ben-Nissan B 2001 Production and analysis of hydroxyapatite from Australian corals via hydrothermal process *Journal of Materials Science Letters* 20 85-7.
[23] Huang S, Zhu J and Zhou K 2012 Effects of Eu3+ ions on the morphology and luminescence properties of hydroxyapatite nanoparticles synthesized by one-step hydrothermal method *Materials Research Bulletin* 47 24–8.
[24] Huang W, Day D E, Kittiratanapiboon K and Rahaman M N 2006 Kinetics and mechanisms of the conversion of silicate (45S5), borate, and borosilicate glasses to hydroxyapatite in dilute phosphate solutions *J. Mater. Sci.: Mater. Med.* 17 583–96.

[25] Hunter G, Kyle C and Goldberg H 1994 Modulat ion of crystal formation by bone phosphoproteins: structural specificity of the osteopontin-mediated inhibition of hydroxyapatite formation *Biochem. J.* 300 723-8.
[26] Ioku K, Kawachi G and Sasaki S 2006 Hydrothermal preparation of tailored hydroxyapatite *J. Mater. Sci.* 41 1341–4.
[27] Ito H, Oaki Y and Imai H 2008 Selective Synthesis of Various Nanoscale Morphologies of Hydroxyapatite via an Intermediate phase *Crystal Growth and Design* 8 1055–9.
[28] Ivankovic H, Ferrer G G, Tkalcec E, Orlic S and Ivankovic M 2009 Preparation of highly porous hydroxyapatite from cuttlefish bone *J. Mater. Sci.: Mater. Med.* 20 1039–46.
[29] Janackovic D, Petrovic-Prelevic I, Kostic-Gvozdenovic L, Petrovic R and Uskokovivc V J D 2001 Influence of synthesis parameters on the particle sizes of nano structured calcium-hydroxyapatite *Key Eng Mater* 203-206 192-5.
[30] Jokanović V, Izvonar D, Dramićanin M D, Jokanović B, Zivojinović V, Marković D and Dacić B 2006 Hydrothermal synthesis and nanostructure of carbonated calcium hydroxyapatite. *J. Mater. Sci. Mater. Med.* 17 539-46.
[31] Juarez-Salinas H, Ott G S, Chen J C, Brooks T L and Stanker L H 1986 Separation of IgG idiotypes by high-performance bydroxylapatite chromatography *Methods Enzymol.* 121 615-22.
[32] Jungbauer A, Hahn R, Deinhofer K and Luo P 2004 Performance and Characterization of a Nanophased Porous Hydroxyapatite for Protein Chromatography *Biotechnology and Bioengineering* 87.
[33] Kawasaki T 1991 Hydroxyapatite as a liquid chromatography packing *J. Chromatogr.* 544 147-84.
[34] Kim B, Langer R and Hrkach J 2000 Biodegradable photo-crosslinked poly (ether-ester) networks for lubricious coatings *Biomaterials* 21 259-65.
[35] Kim S, Ryu H-S, Shin H, Jung H S and Hong K S 2005 In situ observation of hydroxyapatite nanocrystal formation from amorphous calcium phosphate in calcium-rich solutions *Materials Chemistry and Physics* 91 500–6.
[36] Kobayashi T, Ono S, Hirakura S, Oaki Y and Imai H 2012 Morphological variation of hydroxyapatite grown in aqueous solution based on simulated body fluid *Cryst. Eng. Comm.* 12 1143–9.
[37] Koutsoukos P G and Nancollas G H 1981 The morphology of hydroxyapatite crystals grown in aqueous solution at 37°C *Journal of Crystal Growth* 55 369-75.
[38] Kumar M, Dasarathy H and Riley C 1999 Electrodeposition of brushite coatings and their transformation to hydroxyapatite in aqueous solutions *J. Biomed. Mater. Res.* 45 302–10.
[39] Kumar R, Prakash K H, Cheang P and Khor K A 2004 Temperature Driven Morphological Changes of Chemically Precipitated Hydroxyapatite Nanoparticles *Langmuir* 20 5196-200.
[40] Li J, Zhu D, Yin J, Liu Y, Yao F and Yao K 2010 Formation of nano-hydroxyapatite crystal in situ in chitosan–pectin polyelectrolyte complex network *Mater. Sci. Eng. C.* 30 795-803.
[41] Li L, Mao C Y, Wang J M, Xu X R, Pan H H, Deng Y, Gu X H and Tang R K 2011 Bio-Inspired Enamel Repair via Glu-Directed Assembly of Apatite Nanoparticles: an Approach to Biomaterials with Optimal Characteristics *Adv. Mater.* 23 4695-.

[42] Lin K, Chang i and Zhu Y 2011 Facile Synthesis of Hydroxyapatite Nanoparticles, Nanowires and Hollow Nano-structured Microspheres using Similar Structured Hard-precursors *Nanoscale* 3 3052-5.
[43] Lin K, Chang J, Liu X, Chen L and Zhou Y 2011 Synthesis of element-substituted hydroxyapatite with controllable morphology and chemical composition using calcium silicate as precursor *Cryst. Eng. Comm.* 13 4850.
[44] Lin K, Pan J, Chen Y, Cheng R and Xu X 2009 Study the adsorption of phenol from aqueous solution on hydroxyapatite nanopowders *Journal of Hazardous Materials* 161 231-40.
[45] Liu G, Zhao D, Tomsia A P, Minor A M, Song X and Saiz E 2009 Three-Dimensional Biomimetic Mineralization of Dense Hydrogel Templates *J. Am. Chem. Soc.* 131 9937-9.
[46] Liu X, Lin K and Chang J 2011 Modulation of hydroxyapatite crystals formed from a-tricalcium phosphate by surfactant-free hydrothermal exchange *Cryst. Eng. Comm.* 13 1959-65.
[47] Liu Y, Hou D and Wang G 2004 A simple wet chemical synthesis and characterization of hydroxyapatite nanorods *Materials Chemistry and Physics* 86 69-73.
[48] Liu Y K, Wang W Z, Zhan Y J, Zheng C L and Wang G H 2002 A Simple Route to Hydroxyapatite Nanofibers *Mater. Lett.* 56 496-501.
[49] Lu X, Zhang H, Guo Y, Wang Y, Ge X, Leng Y and Wataric F 2011 Hexagonal hydroxyapatite formation on TiO2 nanotubes under urea modulation *Cryst. Eng. Comm.* 13 3741–9.
[50] Luo P and Nieh T G 1996 Preparing hydroxyapatite powders with controlled morphology *Biomaterials* 17 1959-64.
[51] Ma M-G, Zhu Y-J and Chang J 2006 Monetite Formed in Mixed Solvents of Water and Ethylene Glycol and Its Transformation to Hydroxyapatite *J. Phys. Chem. B* 110 14226-30.
[52] Mann S 2001 *Biomineralization: principles and concepts in bioinorganic materials chemistry* (Oxford: Oxford University Press).
[53] Matsumoto T, Okazaki M, Inoue M, Hamada Y, Taira M and Takahashi J 2002 Crystallinity and solubility characteristics of hydroxyapatite adsorbed amino acid *Biomaterials* 23 2241-7.
[54] Milev A, Kannangara G S K and Ben-Nissan B 2003 Morphological stability of hydroxyapatite precursor *Materials Letters* 57 1960–5.
[55] Mizushima Y, Ikoma T, Tanaka J, Hoshi K, Ishihar T, Ogawa Y and Ueno A 2006 Injectable porous hydroxyapatite microparticles as a new carrier for protein and lipophilic drugs *J. Control. Release* 110 260-5.
[56] Mizushima Y, Ikoma T, Tanaka J, Hoshi K, Ishihara T, Ogawa Y and Ueno A 2006 Injectable porous hydroxyapatite microparticles as a new carrier for protein and lipophilic drugs *J. Control. Release* 110 260-5.
[57] Müller F A, Gbureck U, Kasuga T, Mizutani Y, Barralet J E and Lohbauer. U 2007 Whisker reinforced calcium phosphate cements *J. Am. Ceram. Soc.* 90 3694-7.
[58] Nagata F, Yokogawa Y, Toriyama M, Kawamoto Y, Suzuki T and Nishizawa K 1995 Hydrothermal synthesis of hydroxyapatite crystals in the presence of methanol *J. Ceram. Soc. Jpn.* 103 70-3.

[59] Pan H, Liu X Y, Tang R and Xu H Y 2010 Mystery of the transformation from amorphous calcium phosphate to hydroxyapatite *Chem. Comm.* 46 7415-7.
[60] Pieters I Y, Vreken N M F V d, Declercq H A, Cornelissen M J and Verbeeck R M H 2010 Carbonated apatites obtained by the hydrolysis of monetite: Influence of carbonate content on adhesion and proliferation of MC3T3-E1 osteoblastic cells *Acta. Biomaterialia.* 6 1561–8.
[61] Posner A S and Betts F 1975 Synthetic amorphous calcium-phosphate and its relation to bone-mineral structure *Acc. Chem. Res.* 8 273–81.
[62] Raj P, Johnsson M, Levine M and Nancollas G 1992 Salivery statherin: dependence on sequence, charge, hydrogen bonding potency and helical conformation for adsorption to hydroxyapatite and inhibition of mineralization *J. Biol. Chem.* 267 5968-76.
[63] Robinson A 1952 An electron microscopic study of the crystalline inorganic components of bone and its relationship to the organic matrix, *J. Bone Jt. Surg.* 34A 389-434.
[64] Rocha J H G, Lemos A F, Agathopoulos S, Kannan S, Vale′rio P and Ferreira J M F 2006 Hydrothermal growth of hydroxyapatite scaffolds from aragonitic cuttlefish bones *J. Biomed. Mater. Res.* 77A 160-8.
[65] Rocha J H G, Lemos A F, Kannan S, Agathopoulos S and Ferreira J M F 2005 Hydroxyapatite scaffolds hydrothermally grown from aragonitic cuttlefish bones *J. Mater. Chem.* 15 5007-11.
[66] Romberg R, Wernwss P, Riggs B and Mann K 1986 Inhibition of hydroxyapatite crystal growth by bone-specific and other calciumbinding proteins *Biochemistry* 25 1176-11180.
[67] Rubin M, Jasiuk I, Taylor J, Rubin J, Ganey T and Apkarian R 2003 TEM Analysis of the Nanostructure of Normal and Osteoporotic Human Bone *Bone* 33 270-82.
[68] Sadasivan S, Khushalani D and Mann S 2005 Synthesis of calcium phosphate nanofilaments in reverse micelles *Chem. Mater.* 17 2765-70.
[69] Sauer M, Hafele T, Graff A, Nardin C and Meier W 2001 Ion-carrier controlled precipation of calcium phosphate in giant ABA triblock copolymer vesicles *Chem. Commun.* 2453-4.
[70] Schnepp Z A, Gonzalez-McQuire R and Mann S 2006 Hybrid Biocomposites based on Calcium Phosphate Mineralization of Self-assembled Supramolecular Hydrogels *Adv. Mater.* 18 1869-72.
[71] Song J, Malathong V and Bertozzi C R 2005 Mineralization of Synthetic Polymer Scaffolds: A Bottom-Up Approach for the Development of Artificial Bone *J. Am. Chem. Soc.* 127 3366-72.
[72] Song J, Saiz E and Bertozzi C R 2003 A new approach to mineralization of biocompatible hydrogel scaffolds: An efficient process toward 3-dimensional bonelike composites *J. Am. Chem. Soc.* 125 1236-43.
[73] Spanos N, Klepetsanis P G and Koutsoukos P G 2001 Model Studies on the Interaction of Amino Acids with Biominerals: The Effect of L-Serine at the Hydroxyapatite–Water Interface *J. Colloid Interface Sci.* 236 260-5.
[74] Stulajterov R and Medveck L 2008 Effect of calcium ions on transformation brushite to hydroxyapatite in aqueous solutions *Colloids and Surfaces A: Physicochem. Eng. Aspects* 316 104–9.

[75] Su X, Sun K, Cui F Z and Landis W J 2003 Organization of apatite crystals in human woven bone. *Bone* 32 150-62.
[76] Sun R, Lu Y and Chen K 2009 Preparation and characterization of hollow hydroxyapatite microspheres by spray drying method *Mater. Sci. Eng. C* 29 1088-92.
[77] Sun R X, Lu Y P, Li M S, Li S T and Zhu R F 2005 Characterization of hydroxyapatite particles plasma-sprayed into water *Sutf. Coat. Technol.* 190 281-6.
[78] Tao J H, Pan H H, Zeng Y W, Xu X R and Tang R K 2007 Roles of amorphous calcium phosphate and biological additives in the assembly of hydroxyapatite nanoparticles *J. Phys. Chem. B* 111 13410-8.
[79] Taylor H F W 1986 Proposed structure for calcium siliate hydrate gel *J. Am. Ceram. Soc.* 69 464-7.
[80] Tomoda K, Ariizumi H, Nakaji T and Makino K 2010 Hydroxyapatite particles as drug carriers for proteins *Colloids and Surfaces B: Biointerfaces* 76 226-35.
[81] Tornblom M and Henriksson U 1997 Effect of Solubilization of Aliphatic Hydrocarbons on Size and Shape of Rodlike C16TABr Micelles Studied by 2H NMR Relaxation *J. Phys. Chem. B.* 101 6028-35.
[82] Trommer R M, Santos L A and Bergmann C P 2009 Nanostructured hydroxyapatite powders produced by a flame-based technique *Mater. Sci. Eng. C* 29 1770-5.
[83] Wakae H, Takeuchi A, Udoh K, Matsuya S, Munar M L, LeGeros R Z, Nakasima A and Ishikawa K 2008 Fabrication of macroporous carbonate apatite foam by hydrothermal conversion of a-tricalcium phosphate in carbonate solutions *J. Biomed. Mater. Res.* 87A 957–63.
[84] Wang P, Li C, Gong H, Jiang X, Wang H and Li K 2010 Effects of synthesis conditions on the morphology of hydroxyapatite nanoparticles produced by wet chemical process *Powder Technology* 203 315-21.
[85] Wang Q, Huang W, Wang D, Darvell B W, Day D E and Rahaman M N 2009 Strength of hollow hydroxyapatite microspheres prepared by a glass conversion process *J. Mater. Sci.: Mater. Med.* 20 123–9.
[86] Vasiliev A N, Zlotnikov E, Khinast J G and Riman R E 2008 Chemisorption of silane compounds on hydroxyapatites of various morphologies *Scr.Mater.* 58 1029-42.
[87] Weiner S, Arad T and Traub W 1991 Crystal organization in rat bone lamellae *FEBS Lett.* 285 49-54.
[88] Weiner S and Wagner H D 1998 The material bone: structure mechanical function relations *Annu. Rev. Mater. Sci* 28 271-98.
[89] Weng J, Wang M and Chen J 2002 Plasma-sprayed calcium phosphate particles with high bioactivity and their use in bioactive scaffolds *Biomaterials* 23 2623-9.
[90] Vergks M, Fernhdez-Gonzilez C and Martinez-Gallego M 1998 Hydrothermal Synthesis of Calcium Deficient Hydroxyapatites with Controlled Size and Homogeneous Morphology *Journal of Ihe European Ceramic Sociefy* 18 1245-50.
[91] Viswanath B and Ravishankar N 2008 Controlled synthesis of plate-shaped hydroxyapatite and implications for the morphology of the apatite phase in bone *Biomaterials* 29 4855–63.
[92] Wu Y and Hench L L 2004 Preparation of Hydroxyapatite Fibers by Electrospinning Technique *J. Am. Ceram. Soc.* 87 1988–91.
[93] Xin R, Leng Y and Wang N 2006 In situ TEM examinations of octacalcium phosphate to hydroxyapatite transformation *Journal of Crystal Growth* 289 339–44.

[94] Xu J, White T, Li P, He C and Han Y-F 2010 Hydroxyapatite Foam as a Catalyst for Formaldehyde Combustion at Room Temperature *J. Am. Chem. Soc.* 132 13172–3.

[95] Yan L, Li Y, Deng Z-X, Zhuang J and Sun X 2001 Surfactant-assisted hydrothermal synthesis of hydroxyapatite nanorods *International Journal of Inorganic Materials* 3 633-7.

[96] Yang L X, Yin J J, Wang L L, Xing G X, Yin P and Quan-Wen.Liu 2012 Hydrothermal synthesis of hierarchical hydroxyapatite: Preparation, growth mechanism and drug release property *Ceramics International* 38 495–502.

[97] Yang Y, Yao Q Q, Pu X M, Hou Z Q and Zhang Q Q 2011 Biphasic calcium phosphate macroporous scaffolds derived from oyster shells for bone tissue engineering *Chemical Engineering Journal* 173 837-45.

[98] Yao A H, Xu W, Ai F R, Chen Q, Wang D P, Huang W H and Xu J 2011 Study on Hollow Hydroxyapatite Microspheres as Delivery System for Human Bone Morphogenetic Protein *Journal of Inorganic Materials* 26 974-8.

[99] Yoshimura M, Sujaridworakun P, Koh F, Fujiwara T, Pongkao D and Anwar Ahniyaz 2004 Hydrothermal conversion of calcite crystals to hydroxyapatite *Materials Science and Engineering: C* 24 521-5.

[100] Zaremba C M, Morse D E, Mann S, Hansma P K and Stucky G D 1998 Aragonite-Hydroxyapatite Conversion in Gastropod (Abalone) Nacre *Chem. Mater.* 10 3813-24.

[101] Zhang H and Darvell B W 2010 Synthesis and characterization of hydroxyapatite whiskers by hydrothermal homogeneous precipitation using acetamide *Acta. Biomaterialia.* 6 3216-22.

[102] Zhang H G, Zhu Q and Wang Y 2005 Morphologically Controlled Synthesis of Hydroxyapatite with Partial Substitution of Fluorine *Chem. Mater.* 17 5824-30.